

A Convex and Selective Variational Model for Image Segmentation

Jack Spencer* and Ke Chen*[†]

Abstract

Selective image segmentation is the task of extracting one object of interest from an image, based on minimal user input. Recent level set based variational models have shown to be effective and reliable, although they can be sensitive to initialization due to the minimization problems being nonconvex. This sometimes means that successful segmentation relies too heavily on user input or a solution found is only a local minimizer, i.e. not the correct solution. The same principle applies to variational models that extract all objects in an image (global segmentation); however, in recent years, some have been successfully reformulated as convex optimization problems, allowing global minimizers to be found.

There are, however, problems associated with extending the convex formulation to the current selective models, which provides the motivation for the proposal of a new selective model. In this paper we propose a new selective segmentation model, combining ideas from global segmentation, that can be reformulated in a convex way such that a global minimizer can be found independently of initialization. Numerical results are given that demonstrate its reliability in terms of removing the sensitivity to initialization present in previous models, and its robustness to user input.

Keywords. Image processing, Variational segmentation, Level set function, Edge detection, Convex functional, Euler-Lagrange equation, AOS.

AMS subject classifications. 62H35, 65N22, 68U10, 35A15, 65C20, 74G65, 74G75.

1 Introduction

An important part of Image Processing is segmentation; the task of partitioning an image into multiple regions (each sharing certain characteristics - such as texture, intensity, shape, colour etc.). Given an image $z(x, y)$ in a bounded domain $\Omega \subset \mathbb{R}^2$, we look for an edge Γ that partitions Ω into regions $\{\Omega_i, i = 1, 2, \dots, l\}$ in $\Omega \setminus \Gamma$. Within Segmentation, there is the global approach and the local approach. Global segmentation is the task of selecting all objects in an image based on a certain characteristic, e.g. intensity, and has been widely studied over the last twenty years [9, 21]. Selective segmentation is when only one object, from within all objects, is selected [1, 27].

*Centre for Mathematical Imaging Techniques and Department of Mathematical Sciences, University of Liverpool, United Kingdom. Email: cmit@liverpool.ac.uk, Web: www.liv.ac.uk/cmit

[†]Corresponding author. Email: k.chen@liv.ac.uk

We consider the variational approach to these problems. Within variational segmentation techniques two main ideas have developed: edge-based methods and region-based methods. An important region-based method, where the idea is to achieve segmentation through an approximation of the original image, is the Mumford-Shah functional minimization [22]; there exists a large literature extending this work. Edge-based methods drive an evolving contour towards edges within an image using an edge detector function. This method was originally proposed by Kass et al. [17]; further work by Caselles et al. led to the Geodesic Active Contours model [5]. Recently, in order to incorporate the advantages of each idea, there has been a tendency to combine edge-based and region-based approaches [19, 5].

The requirements for a selective segmentation model are that solutions are computed quickly and they are reliable with minimal user input. Much research has been done in recent years on developing this idea. In 2005, Gout, Le Guyader and Vese [14] introduced geometrical constraints to Geodesic Active Contours similar to [5] in the form of a set of points on the contour of interest. This idea was enhanced further by Badshah and Chen [1] in 2009, by combining this work with the region-based idea of Mumford-Shah [22] and Chan-Vese [10]. In 2011, to increase model reliability, Rada et al. [27] introduced a novel Dual Level Set Model, where a local level set incorporates geometrical constraints similar to [14] and [1], locating an object within a global level set. The selective model discussed in detail here is the Rada-Chen model [28], introduced in 2012 to improve on [27] by using a single level set function, where there is a constraint introduced on the area inside the contour. This has proven to be the most effective model. Another idea of improving [1], that is not of the same type as [22], was proposed by Badshah and Chen [2] in 2012, incorporating fitting based on coefficient of variation.

These models, either global or selective, are nonconvex, which can lead to problems in the form of local minima. This means that finding the correct solution is dependent on initialization, which reduces their reliability. In recent years work has been done to reformulate global segmentation models as convex minimization problems such that any local minimizer is a global minimizer. The focus of this paper is to apply the convex reformulation of nonconvex global models to selective segmentation. We remark that one of the current challenges in global segmentation is reformulation into convex or relaxed models for multiphase cases [18, 15, 6, 3]. Other challenges include the idea of selective segmentation based on user input of 3-D images. Chan-Vese has been generalized to 3-D by Zhang and Chen [31], and user input of a similar type to [1, 28, 14] has been applied with active contours in 3-D by Le Guyader and Gout [13]. This involves the selection of points on slices of the 3-D data. Visualising objects in this way, allowing for efficient user input, is a difficult problem. In relation to Rada-Chen [28], this input would generate a polyhedron, with its volume providing a selection constraint.

The paper is organized as follows. In Section 2 the idea of global segmentation is discussed, including brief reviews of the work of Mumford-Shah [22], Chan-Vese [10] and Chan-Esedoglu-Nikilova [8]. This will detail how nonconvex segmentation models are reformulated as convex minimization problems. In Section 3 selective segmentation is discussed with a review of the most effective model by Rada-Chen [28]. Why this model does not fit in with the convex reformulation idea is explained, motivating the proposal of a new model in Section 4. The details of this model are discussed in the nonconvex setting and then reformulated as a convex minimization problem. Details of an adjusted additive operator splitting (AOS) scheme, based on Weickert et al. [29] and Tai. et al. [20], are also introduced. Section 5 presents results for

both the nonconvex and convex models. Conclusions of the paper are given in Section 6.

2 Global Segmentation

In order to discuss the selective segmentation methods of interest, it is important to introduce global variational image segmentation models. This is important for two reasons; firstly, it will provide the foundation for the selective models introduced and secondly, it provides the method for minimizing the associated functionals with the introduction of Active Contours Without Edges [10] by Chan and Vese in 2001.

2.1 The Mumford-Shah Approach

One of the most important variational image segmentation models is by Mumford and Shah [22], introduced in 1989, and forms the basis for this work as well as many others. Let Ω be a bounded domain in \mathbb{R}^n and z be a bounded measurable function defined on Ω . Here we consider the case where $n = 2$. In the piecewise constant case, the image, z , is reconstructed as a cartoon of the original where each region, Ω_i , consists of homogeneous intensity (with $i = 1, \dots, l$), separated by an edge set Γ , a closed subset of Ω .

In 2001, Chan and Vese [10] introduced a particular case of the piecewise constant Mumford-Shah functional. This was the two-phase example ($l = 2$), with $\Omega_1 = \text{in}(\Gamma)$ and $\Omega_2 = \text{out}(\Gamma)$, which looks for the best approximation of an image z by a function u taking only 2 values,

$$u = \begin{cases} c_1 = \text{average of } z \text{ inside } \Gamma, \\ c_2 = \text{average of } z \text{ outside } \Gamma. \end{cases}$$

The length of the set Γ is given by

$$|\Gamma| = \int_{\Gamma} ds.$$

The piecewise constant two-phase Mumford-Shah (*PC*) functional is given as follows:

$$PC(\Gamma, c_1, c_2) = \mu|\Gamma| + \lambda \int_{\text{in}(\Gamma)} (z - c_1)^2 d\Omega + \lambda \int_{\text{out}(\Gamma)} (z - c_2)^2 d\Omega. \quad (2.1)$$

It consists of the regularization term, $|\Gamma|$, forcing the boundary between homogeneous regions to be as short and as smooth as possible, and the fitting terms which force the boundary to find regions of homogeneous intensity. Theoretical existence and regularity of minimizers of the *PC* case (2.1), with respect to Γ , are discussed in [22]. However, minimizing *PC* (2.1) is problematic due to the difficulty of tracking the movement of Γ and the model was not implemented directly until the work of [10].

2.2 The Chan-Vese Method

Active Contours Without Edges [10], by Chan and Vese, is an important milestone in variational image segmentation. They applied the level set method to minimize the piecewise constant two-phase Mumford-Shah functional, eqn. (2.1), and overcame the problematic tracking of Γ . Chan

and Vese proposed to replace the unknown 1-D variable with a higher dimensional variable, counterintuitively simplifying the problem. They applied the level set method [26], introduced by Osher and Sethian in 1988, to (2.1). By tracking a variable of a higher dimension, where the boundary is represented by a level set of this variable, topological changes in the boundary, such as splitting into two or merging into one, are dealt with automatically. Formally, the boundary Γ is represented by the zero level set of the Lipschitz function ϕ such that

$$\begin{cases} \Gamma = \{(x, y) \in \Omega \mid \phi(x, y) = 0\}, \\ \text{in}(\Gamma) = \{(x, y) \in \Omega \mid \phi(x, y) > 0\}, \\ \text{out}(\Gamma) = \{(x, y) \in \Omega \mid \phi(x, y) < 0\}. \end{cases}$$

The *PC* functional (2.1) is reformulated using the Heaviside function H and the Dirac delta δ defined by

$$H(\phi(x, y)) = \begin{cases} 1, & \text{if } \phi(x, y) \geq 0 \\ 0, & \text{if } \phi(x, y) < 0, \end{cases} \quad \delta(\phi(x, y)) = H'(\phi(x, y)).$$

In order to compute the associated Euler-Lagrange (EL) equation for ϕ we consider regularized versions of H and δ , given as

$$H_\epsilon(\phi) = \frac{1}{2} \left(1 + \frac{2}{\pi} \arctan \frac{\phi}{\epsilon} \right), \quad \delta_\epsilon(\phi) = \frac{1}{\epsilon\pi(1 + \phi^2/\epsilon^2)}.$$

The *PC* functional (2.1) is then reformulated as follows:

$$\begin{aligned} CV(\phi, c_1, c_2) = \mu \int_{\Omega} \delta(\phi) |\nabla H_\epsilon(\phi)| d\Omega + \lambda \int_{\Omega} (z - c_1)^2 H_\epsilon(\phi) d\Omega \\ + \lambda \int_{\Omega} (z - c_2)^2 (1 - H_\epsilon(\phi)) d\Omega, \end{aligned} \quad (2.2)$$

where $\phi(x, y)$ has been replaced with ϕ for simplicity; this notation will be continued from here. Minimizing (2.2) with respect to the intensity constants c_1 and c_2 is given by:

$$c_1(\phi) = \frac{\int_{\Omega} H_\epsilon(\phi) z d\Omega}{\int_{\Omega} H_\epsilon(\phi) d\Omega}, \quad c_2(\phi) = \frac{\int_{\Omega} (1 - H_\epsilon(\phi)) z d\Omega}{\int_{\Omega} (1 - H_\epsilon(\phi)) d\Omega}. \quad (2.3)$$

Then, given these constants, (2.2) is minimized with respect to ϕ :

$$\min_{\phi} CV(\phi, c_1, c_2) \quad (2.4)$$

This leads to the EL equation

$$\begin{cases} \mu \delta_\epsilon(\phi) \nabla \cdot \left(\frac{\nabla \phi}{|\nabla \phi|} \right) - \lambda \delta_\epsilon(\phi) \left((z - c_1)^2 - (z - c_2)^2 \right) = 0 & \text{in } \Omega, \\ \frac{\partial \phi}{\partial \vec{n}} = 0 & \text{on } \partial\Omega. \end{cases}$$

The work of Chan and Vese is important to the consideration of selective segmentation as it provides the method to tackle segmentation problems of this type in an efficient way. It does however have a drawback in that it involves minimizing a nonconvex functional (2.2) over

characteristic functions. This means that there are local minima and a computed solution may not be correct unless the initial guess is sufficiently close to the true solution. Fortunately, by reformulating as the minimization of a convex functional, global minimizers of the nonconvex problem (2.4) can be found. This idea has not yet been applied to selective segmentation models, which also have local minima.

2.3 A Global Convex Reformulation

Important to the idea of reformulating a model to be convex is why this improves the reliability of a solution. With that in mind, the fundamental idea behind convex minimization is now discussed briefly in a general sense. Consider the problem of minimizing $f(\mathbf{x})$ subject to $\mathbf{x} \in S$, given a non-empty set S . A point $\mathbf{x} \in S$ is called a feasible solution to the problem. If $\bar{\mathbf{x}} \in S$ and $f(\mathbf{x}) \geq f(\bar{\mathbf{x}})$ for each $\mathbf{x} \in S$, then $\bar{\mathbf{x}}$ is a global minimum. If $\bar{\mathbf{x}} \in S$ and there exists an ϵ -neighbourhood $N_\epsilon(\bar{\mathbf{x}})$ around $\bar{\mathbf{x}}$ such that $f(\mathbf{x}) \geq f(\bar{\mathbf{x}})$ for each $\mathbf{x} \in S \cap N_\epsilon(\bar{\mathbf{x}})$, then $\bar{\mathbf{x}}$ is called a local minimum.

The advantage of convex minimization is that supposing $\bar{\mathbf{x}}$ is a local minimum, if f is convex and S is a convex set, then $\bar{\mathbf{x}}$ is a global minimum. It has been shown that minimizing the piecewise constant two-phase Mumford-Shah functional with respect to Γ can be reformulated as a convex problem, by relaxation of the label set. We now introduce the theory behind reformulating the functional (2.1), which we shall later apply to selective segmentation.

We consider the minimization of the piecewise constant two-phase Mumford-Shah functional from (2.1) with respect to Γ ; reformulated to the minimization problem (2.4) by Chan and Vese [10]. Observe that

$$CV(\phi, c_1, c_2) = \mu \int_{\Omega} \delta(\phi) |\nabla H(\phi)| d\Omega + \lambda \int_{\Omega} (z - c_1)^2 H(\phi) d\Omega + \lambda \int_{\Omega} (z - c_2)^2 (1 - H(\phi)) d\Omega$$

is nonconvex due to the presence of $H(\phi)$. In 2006, Chan, Esedoglu and Nikilova [8] proposed replacing $H(\phi)$ with $u \in [0, 1]$ in (2.2), and obtained the following equivalent, convex, and constrained minimization problem:

$$\min_{0 \leq u \leq 1} \left\{ \mu \int_{\Omega} |\nabla u| d\Omega + \lambda \int_{\Omega} ((z - c_1)^2 - (z - c_2)^2) u d\Omega \right\}. \quad (2.5)$$

Here the constraint $0 \leq u \leq 1$ ensures that u is a valid Heaviside function and the equivalence to Chan-Vese is in the sense of having the same EL equation. For any fixed $c_1, c_2 \in \mathbb{R}^+$, a global minimizer for $CV(\cdot, c_1, c_2)$ can be found by carrying out the convex minimization (2.5) [8]. Once the solution u is obtained, set $\Sigma = \{(x, y) : u(x, y) \geq \gamma\}$ for $\gamma \in (0, 1)$ and then in terms of piecewise-constant two-phase Mumford-Shah, $\Gamma = \partial\Sigma$. As remarked, the convex problem (2.5) will find a global minimizer independently of the initial guess for u .

3 The Selective Segmentation Problem and Recent Models

The task of extracting only one object from an image is a challenging problem within segmentation with applications in a number of areas, such as automated object detection in security

monitoring and feature selection in medical imaging. Within medical applications, advances in this subject can improve quantitative diagnosis, help monitor treatment over time and improve pre-operative planning.

Here, on image z , we assume the availability of $n_1 (\geq 3)$ points inside the target object that form a set $\mathcal{A} = \{w_i = (x_i^*, y_i^*) \in \Omega, 1 \leq i \leq n_1\}$ that defines a polygon. A common misconception is that if \mathcal{A} is available any global, nonconvex model (such as [10]) can solve the selective segmentation problem if one places the initial contour of ϕ near \mathcal{A} . Indeed, this is true for some simple and designed images where features in an image are distinct, but in general this idea does not lead to a useful method for selective segmentation. We also remark that our problem setting is not the same as that of using seeds for fuzzy membership approaches [24, 32]. One model recently proposed by Nguyen et al. [25] attempts another kind of selective segmentation in a similar way and works with a marker set \mathcal{A} and another ‘anti-marker’ set \mathcal{B} which contains points not within the object to be extracted. It uses an edge detector and a probability map, based on user input, but its results tend to be too dependent on user input.

In order for a selective method to be suitable in this context, it is imperative that a model requires minimal user input and is reliable. Recent developments in the subject include Gout et al. [14], Badshah-Chen [1] and Rada et al. [27], which include region, edge and geometrical constraints. The geometrical constraints are used to modify the regularization term by a distance function, for instance the following used in [1],

$$d(x, y) = \text{distance}((x, y), \mathcal{A}) = \prod_{i=1}^{n_1} \left(1 - e^{-\frac{(x - x_i^*)^2}{2\kappa^2}} e^{-\frac{(y - y_i^*)^2}{2\kappa^2}} \right), \quad \forall (x, y) \in \Omega, \quad (3.1)$$

where κ is a positive constant. Alternative distance functions are also possible. It is also possible to alter the regularization term with the addition of an edge detector (as in [5]), where the strength of detection is adjusted by a parameter, β :

$$g(|\nabla z|) = \frac{1}{1 + \beta |\nabla z|^2}. \quad (3.2)$$

These additions modify the regularization term [27, 1] to be:

$$\int_{\Gamma} d \cdot g \, ds.$$

Of the selective models studied, two effective models capable of segmenting a wide range of examples in a robust way are by Rada-Chen [28] (based on area constraints) and Badshah-Chen [2] (based on non- L_2 fitting). Here "robust" means that correct segmentations have been obtained as long as the initial contour is strictly inside the object to be extracted.

As with Chan-Vese, these selective models are nonconvex. This means that the models can find local minima, depending on the initialization of the contour (which are associated with initial contours not strictly within the object to be extracted). This lack of convexity is problematic for a selective segmentation model as reliability and consistency are key in possible applications.

Our intention is to introduce a new nonconvex selective model and reformulate it as a convex minimization problem, in order to compute the original model’s global minimizer. Our

candidates are Rada-Chen [28] and Badshah-Chen [2]. The fitting terms of [2] are based on the coefficient of variation rather than the mean intensity, used in [22, 10]. The convex reformulation idea from Chan et al. [8] was applied to mean intensity fitting terms, so we intend to focus on Rada-Chen [28] (which also uses mean intensity). Also, the geometrical constraints (3.1) used in [2] can sometimes be too weak based on simple user input, whereas Rada-Chen [28] is less sensitive to the choice of \mathcal{A} . The area constraint of Rada-Chen [28] is an addition to Chan-Vese [10], but is also unsuitable for the convex reformulation. We intend to discuss the reasons for the lack of suitability in further detail. We provide important details of Rada-Chen [28] below, to demonstrate why the convex reformulation fails here.

From the polygon formed by the marker set \mathcal{A} , denote by A_1 and A_2 respectively the area inside and outside the polygon. The Rada-Chen model [28] makes use of A_1 and A_2 to achieve selective segmentation. The initial contour starts from a polygon inside the object and the additional terms restrict the area inside Γ from growing larger than the target object (and therefore outside the object boundary). It also incorporates the edge detector (3.2) into the regularization term. We denote the weighted regularization term as

$$|\Gamma|_g = \int_{\Gamma} g(|\nabla z|) ds.$$

These additions to the piecewise-constant two-phase Mumford-Shah functional (2.1) give us the following energy for selective segmentation:

$$\begin{aligned} RC(\Gamma, c_1, c_2) = & \mu |\Gamma|_g + \lambda \int_{\text{in}(\Gamma)} (z - c_1)^2 dx dy + \lambda \int_{\text{out}(\Gamma)} (z - c_2)^2 dx dy \\ & + \frac{\theta}{2} \left[\left(\int_{\text{in}(\Gamma)} d\xi d\eta - A_1 \right)^2 + \left(\int_{\text{out}(\Gamma)} d\xi d\eta - A_2 \right)^2 \right]. \end{aligned} \quad (3.3)$$

Using the level set formulation, this energy (3.3) becomes [28]:

$$\begin{aligned} RC(\phi, c_1, c_2) = & \mu \int_{\Omega} g(|\nabla z|) \delta(\phi) |\nabla H(\phi)| dx dy \\ & + \lambda \int_{\Omega} (z - c_1)^2 H(\phi) dx dy + \lambda \int_{\Omega} (z - c_2)^2 (1 - H(\phi)) dx dy \\ & + \frac{\theta}{2} \left[\left(\int_{\Omega} H(\phi) d\xi d\eta - A_1 \right)^2 + \left(\int_{\Omega} (1 - H(\phi)) d\xi d\eta - A_2 \right)^2 \right]. \end{aligned} \quad (3.4)$$

The energy is minimized successively with respect to the intensity constants, c_1 and c_2 given by (2.3), and ϕ . The nonconvex problem of minimizing (3.4) with respect to ϕ ,

$$\min_{\phi} RC(\phi, c_1, c_2) \quad (3.5)$$

leads to the EL equation, where $g = g(|\nabla z|)$,

$$\begin{cases} \mu \delta_{\epsilon}(\phi) \nabla \cdot \left(g \frac{\nabla \phi}{|\nabla \phi|} \right) + f = 0 & \text{in } \Omega, \\ \frac{\partial \phi}{\partial \bar{n}} = 0 & \text{on } \partial \Omega, \end{cases} \quad (3.6)$$

$$\text{and} \quad f = -\lambda \delta_\epsilon(\phi) \left\{ (z - c_1)^2 - (z - c_2)^2 \right\} \\ - \theta \delta_\epsilon(\phi) \left\{ \left(\int_\Omega H_\epsilon(\phi) d\Omega - A_1 \right) - \left(\int_\Omega (1 - H_\epsilon(\phi) d\Omega - A_2) \right) \right\}.$$

Solving (3.6) can be done with the introduction of an artificial time step and using the gradient descent method:

$$\frac{\partial \phi}{\partial t} = \mu \delta_\epsilon(\phi) \nabla \cdot \left(g \frac{\nabla \phi}{|\nabla \phi|} \right) + f.$$

We now discuss the possibility of reformulating (3.5) into a convex minimization problem. There are two reasons which mean this is not possible, which have to be considered for the proposal of an appropriate model. Firstly, the additional terms, based on A_1 and A_2 , only incorporate the area of the object into the functional (3.4). This means that information about the location of the object is provided by the initialization. Clearly, convex reformulation where a global minimizer is found independently of initialization is not feasible in this case. Secondly, the method of convex reformulation of Chan et al. [8] introduced above requires linearity in $H(\phi)$, in the fitting term of (3.4). The area constraint of Rada-Chen [28] violates this condition. This provides the two main considerations in proposing a new selective model, suitable for convex reformulation, which we detail next.

4 The Proposed Model

In the following is the introduction of our new model that fits in with the idea of being reformulated as a convex minimization problem and is broadly speaking analogous to Rada-Chen [28]. It uses the same user input as [28], whilst instead of penalizing the area inside the contour from growing too much, it penalizes the contour from moving further away from the polygon, a set of points denoted by \mathcal{P} , formed by the user input set, \mathcal{A} . The new constraint is linear in the indicator function and includes locational information of the target object, consistent with the idea of convex reformulation.

4.1 A New Nonconvex Selective Model

The proposed nonconvex model, to be called Distance Selective Segmentation (DSS), has a different area fitting term than Rada-Chen [28]. The function $P_d(x, y)$ is the normalized Euclidean distance of each point $(x, y) \in \Omega$ from its nearest point in the polygon, made up of $(x_p, y_p) \in \mathcal{P}$, constructed from the user input set, \mathcal{A} :

$$P_0(x, y) = \sqrt{(x - x_p)^2 + (y - y_p)^2}, \\ P_d(x, y) = \frac{P_0(x, y)}{\|P_0\|_{L^\infty}}. \quad (4.1)$$

The DSS functional is then defined as:

$$\begin{aligned}
DSS(\Gamma, c_1, c_2) &= \mu|\Gamma|_g + \theta \int_{\text{in}(\Gamma)} P_d(x, y) d\Omega \\
&+ \lambda \int_{\text{in}(\Gamma)} (z - c_1)^2 d\Omega + \lambda \int_{\text{out}(\Gamma)} (z - c_2)^2 d\Omega.
\end{aligned} \tag{4.2}$$

Here, we have the regularization and fitting terms from the piecewise constant two-phase Mumford-Shah functional (2.1) with the addition of a new distance fitting term, normalized so that $P_d(x, y) \in [0, 1]$. For $(x, y) \in \mathcal{P}$, $P_d(x, y) = 0$ and (4.2) reduces to (2.1), except the regularization term is weighted by an edge detector function (3.2) as in [4, 28]. Introducing the level set formulation, (4.2) reduces to the following model:

$$\begin{aligned}
\min_{\phi, c_1, c_2} \left\{ DSS^{LS}(\phi, c_1, c_2) &= \mu \int_{\Omega} \delta_{\epsilon}(\phi) g |\nabla \phi| + \theta \int_{\Omega} H_{\epsilon}(\phi) P_d d\Omega \right. \\
&+ \lambda \int_{\Omega} H_{\epsilon}(\phi) (z - c_1)^2 d\Omega + \lambda \int_{\Omega} (1 - H_{\epsilon}(\phi)) (z - c_2)^2 d\Omega \left. \right\}, \tag{4.3}
\end{aligned}$$

Here, if the area parameter, θ , is too strong the final result will just be the polygon \mathcal{P} which of course is undesirable. The idea behind the P_d term is that it encourages $H(\phi) \in \Omega \setminus \mathcal{P}$ to be 0, enforced more strictly the further from the object of interest a point is. The motivation behind this new model is that it fits in with the idea of convex reformulation.

But it is important to clarify whether the idea behind this segmentation model, i.e. the distance constraint, works as it is. The answer is yes. Comparisons of (4.3) with Rada-Chen [28] are made for three examples and shown in Figures 1-2 of Section 5.1. There, one clearly observes that the two sets of segmentation results are successful. That is, (4.3) is a valid selective segmentation in its own right. In the third example, where the initial guess is altered, both results are unsuccessful as local minima have been found. We look to correct this fault in DSS (4.3) by convexification of the model.

4.2 A Selective Convex Reformulation

We now present details for the convex reformulation of (4.3). As in [8] the DSS^{LS} energy can be made convex by making the adjustment $H_{\epsilon}(\phi) \rightarrow u \in [0, 1]$ to give the Convex Distance Selective Segmentation (CDSS) functional:

$$CDSS(u, c_1, c_2) = \mu \int_{\Omega} |\nabla u|_g d\Omega + \lambda \int_{\Omega} r u d\Omega + \theta \int_{\Omega} P_d u d\Omega \tag{4.4}$$

where $r = (z - c_1)^2 - (z - c_2)^2$ and $|\nabla u|_g = g(|\nabla z|)|\nabla u|$. Given initial values for c_1 and c_2 , based on the set \mathcal{A} , our model consists of the following constrained minimization problem:

$$\min_{0 \leq u \leq 1} CDSS(u, c_1, c_2). \tag{4.5}$$

Define $\Sigma = \{(x, y) : u(x, y) \geq \gamma\}$ for $\gamma \in (0, 1)$. Following the work of Chan et al. [8], we can demonstrate that a minimizer for DSS (4.3) is given by (4.5). Using the Coarea formula [11],

for the first term, the weighted total variation (TV) norm, in (4.2), we get

$$\begin{aligned} \int_{\Omega} |\nabla u|_g d\Omega &= \int_0^1 g(|\nabla z|) \text{Per}\left(\{(x, y) : u(x, y) \geq \gamma\}; \Omega\right) d\gamma \\ &= \int_0^1 g(|\nabla z|) \text{Per}\left(\Sigma(\gamma); \Omega\right) d\gamma = \int_0^1 |\Gamma|_g d\gamma. \end{aligned} \quad (4.6)$$

For the remaining terms in (4.2) we first need to introduce a definition. Let u be a non-negative, real-valued, measurable function on Ω . Then with χ a characteristic function,

$$u(x) = \int_0^\infty \chi_{u(x) > t} dt.$$

For the first fitting term, as $u \in [0, 1]$, we have

$$\begin{aligned} \int_{\Omega} (z - c_1)^2 u d\Omega &= \int_{\Omega} (z - c_1)^2 \int_0^1 \chi_{\Sigma(\gamma)} d\gamma d\Omega = \int_0^1 \int_{\Omega} (z - c_1)^2 \chi_{\Sigma(\gamma)} d\Omega d\gamma \\ &= \int_0^1 \int_{\Sigma(\gamma)} (z - c_1)^2 d\Omega d\gamma, \end{aligned} \quad (4.7)$$

and for the other two terms, similarly, we have

$$\int_{\Omega} (z - c_2)^2 u d\Omega = \int_0^1 \int_{\Sigma(\gamma)} (z - c_2)^2 d\Omega d\gamma = C - \int_0^1 \int_{\Omega \setminus \Sigma(\gamma)} (z - c_2)^2 d\Omega d\gamma, \quad (4.8)$$

$$\int_{\Omega} P_d u d\Omega = \int_0^1 \int_{\Sigma(\gamma)} P_d d\Omega d\gamma, \quad (4.9)$$

where $C = \int_{\Omega} (z - c_2)^2 d\Omega$ and is independent of u . Combining equations (4.6)-(4.9):

$$\begin{aligned} CDSS(u, c_1, c_2) &= \int_0^1 \left\{ |\Gamma|_g + \lambda \int_{\Sigma(\gamma)} (z - c_1)^2 d\Omega \right. \\ &\quad \left. + \lambda \int_{\Omega \setminus \Sigma(\gamma)} (z - c_2)^2 d\Omega + \theta \int_{\Sigma(\gamma)} P_d d\Omega \right\} d\gamma - C \\ &= \int_0^1 DSS(\Gamma, c_1, c_2) d\gamma - C. \end{aligned}$$

Since C is independent of u , it follows that if u is a minimizer of $CDSS(\cdot, c_1, c_2)$ then for $\gamma \in (0, 1)$ the set $\Gamma = \Sigma(\gamma)$ is a minimizer of $DSS(\cdot, c_1, c_2)$. However, the convex minimization problem (4.5) will provide us with the ability to find a global minimizer, independently of initialization.

4.3 Unconstrained Minimization

The constrained minimization problem (4.5) can be replaced by an unconstrained one:

$$\min_u \left\{ CDSS(u, c_1, c_2) = \mu \int_{\Omega} |\nabla u|_g d\Omega + \int_{\Omega} ru d\Omega + \theta \int_{\Omega} P_d u d\Omega + \alpha \int_{\Omega} \nu(u) d\Omega \right\}$$

where $\nu(u) = \max\{0, 2|u - 1/2| - 1\}$ is an exact penalty term [16], provided that $\alpha > \frac{1}{2}\|\lambda r + \theta P_d\|_{L^\infty}$ (see a proof in [8] for a related problem). In order to compute the associated EL equation for u we introduce a regularized version of the penalty function, $\nu_{\epsilon_1}(u)$:

$$\nu_{\epsilon_1}(u) = H_{\epsilon_1}\left(\sqrt{(2u-1)^2 + \epsilon_1} - 1\right)\left[\sqrt{(2u-1)^2 + \epsilon_1} - 1\right],$$

where $H_{\epsilon_1}(x) = \frac{1}{2}\left(1 + \frac{2}{\pi} \arctan \frac{x}{\epsilon_1}\right)$. Then we get the following EL equation for u :

$$\begin{cases} \mu \nabla \cdot \left(g \frac{\nabla u}{|\nabla u|}\right) - \lambda r - \theta P_d - \alpha \nu'_{\epsilon_1} = 0 & \text{in } \Omega, \\ \frac{\partial u}{\partial \vec{n}} = 0 & \text{on } \partial\Omega. \end{cases} \quad (4.10)$$

To minimize for the intensity values, we use the following equations:

$$c_1(u) = \frac{\int_{\Omega} uz \, d\Omega}{\int_{\Omega} u \, d\Omega}, \quad c_2(u) = \frac{\int_{\Omega} (1-u)z \, d\Omega}{\int_{\Omega} (1-u) \, d\Omega}. \quad (4.11)$$

4.4 Numerical Aspects

Equation (4.10) can be solved by the gradient descent method by solving the following:

$$\frac{\partial u}{\partial t} = \mu \nabla \cdot \left(\frac{g \nabla u}{|\nabla u|}\right) \underbrace{-\lambda r - \theta P_d - \alpha \nu'_{\epsilon_1}}_f. \quad (4.12)$$

One option to solve (4.12) is an explicit scheme, which is computationally cheap but stability conditions often lead to a very restricted time step, τ . The resulting system of equations from a semi-implicit scheme is laborious to solve. This means that neither method is suitable for a model where computational speed is required. Instead we apply the semi-implicit additive operator splitting (AOS) proposed by [20, 29]. To avoid singularities we replace $|\nabla u|$ with $|\nabla u|_{\epsilon_2} = \sqrt{u_x^2 + u_y^2 + \epsilon_2}$ for small ϵ_2 , and denote $W = \frac{g}{|\nabla u|_{\epsilon_2}}$. Freezing W linearizes the equation and (4.12) can be rewritten in the form:

$$\frac{\partial u}{\partial t} = \mu \left(\partial_x (W \partial_x u) + \partial_y (W \partial_y u) \right) + f$$

After discretization rewrite in the matrix-vector form ($\hat{u}^n = u^n + \tau f$):

$$u^{n+1} = \frac{1}{2} \sum_{\ell=1}^2 (I - 2\tau\mu A_\ell(u^n))^{-1} \hat{u}^n. \quad (4.13)$$

Here, A_ℓ is the diffusion quantity in the ℓ direction ($\ell = 1, 2$ for x and y directions respectively) and was derived using the finite difference method, τ is the time step size and n denotes the n^{th} iteration. The matrices A_ℓ are given as follows, where $W_{ij}^n = W(u_{ij}^n)$, and h_x and h_y are

the grid sizes in the x and y directions respectively:

$$\begin{aligned}
\left(A_1(u^n)u^{n+1}\right)_{i,j} &= \left(\partial_x(W^n \partial_x u^{n+1})\right)_{i,j} \\
&= \frac{1}{h_x} \left(W_{i+1/2,j}^n (\partial_x u^{n+1})_{i+1/2,j} - W_{i-1/2,j}^n (\partial_x u^{n+1})_{i-1/2,j} \right) \\
&= \frac{1}{h_x} \left(\frac{W_{i+1,j}^n + W_{i,j}^n}{2} \left(\frac{u_{i+1,j}^{n+1} - u_{i,j}^{n+1}}{h_x} \right) - \frac{W_{i,j}^n + W_{i-1,j}^n}{2} \left(\frac{u_{i,j}^{n+1} - u_{i-1,j}^{n+1}}{h_x} \right) \right) \\
&= u_{i+1,j}^{n+1} \left(\frac{W_{i+1,j}^n + W_{i,j}^n}{2h_x^2} \right) + u_{i-1,j}^{n+1} \left(\frac{W_{i-1,j}^n + W_{i,j}^n}{2h_x^2} \right) \\
&\quad - u_{i,j}^{n+1} \left(\frac{W_{i+1,j}^n + W_{i-1,j}^n + 2W_{i,j}^n}{2h_x^2} \right)
\end{aligned}$$

and similarly,

$$\begin{aligned}
\left(A_2(u^n)u^{n+1}\right)_{i,j} &= \left(\partial_y(W^n \partial_y u^{n+1})\right)_{i,j} = u_{i,j+1}^{n+1} \left(\frac{W_{i,j+1}^n + W_{i,j}^n}{2h_y^2} \right) + u_{i,j-1}^{n+1} \left(\frac{W_{i,j-1}^n + W_{i,j}^n}{2h_y^2} \right) \\
&\quad - u_{i,j}^{n+1} \left(\frac{W_{i,j+1}^n + W_{i,j-1}^n + 2W_{i,j}^n}{2h_y^2} \right).
\end{aligned}$$

The benefits of this method are that at each iteration the solution to two tridiagonal linear systems is required, which can be computed efficiently with the Thomas Algorithm [29, pp.5-6]. However, the original AOS method described above generally assumes f is not dependent on u . Actually, in our case, the term $\nu'_\epsilon(u)$ in f does depend on u , which can lead to stability restrictions in practice. This prompts us to consider an extension of the original AOS, to improve performance and ensure stability of the scheme.

4.4.1 An Improved AOS Method

The changes in f in (4.12) between iterations result in stability restrictions on τ . The shape of $\nu'_\epsilon(u)$ means that changes are problematic near $u = 0$ and $u = 1$, as small changes in u produce large changes in f . In order to overcome this, we define an interval I_ϵ , where we adjust the equation based on the linear part of $\nu'_\epsilon(u)$ and the difference in u between iterations. This minimizes the changes in f from n to $n + 1$. We will demonstrate the adjustments made by first looking at the equation in the x -direction, $\ell = 1$ (similar for the y -direction, $\ell = 2$), for the original AOS scheme [29], that we will call AOS_0 from here. Denoting

$$\bar{f}^n = -\tau\alpha\nu'_\epsilon(u^n) - \tau(\theta P_d + \lambda r):$$

$$\begin{aligned} \frac{\partial u_1}{\partial t} &= \mu \nabla \cdot \left(\frac{\nabla u_1^{n+1}}{|\nabla u_1^{n+1}|_{\epsilon_2}} \right) + \frac{f}{2} \\ \frac{u_1^{n+1} - u_1^n}{2\tau} &= \mu \nabla \cdot \left(\frac{\nabla u_1^{n+1}}{|\nabla u_1^{n+1}|_{\epsilon_2}} \right) + \frac{f}{2} \\ u_1^{n+1} &= u_1^n + 2\tau\mu \nabla \cdot \left(\frac{\nabla u_1^{n+1}}{|\nabla u_1^{n+1}|_{\epsilon_2}} \right) + \bar{f}^n \\ (I - 2\tau\mu A(u_1^n)) u_1^{n+1} &= u_1^n + \bar{f}^n \\ u_1^{n+1} &= \underbrace{(I - 2\tau\mu A(u_1^n))^{-1}}_{Q_0} (u_1^n + \underbrace{\bar{f}^n}_{f_0}). \end{aligned} \quad (4.14)$$

We make an adjustment to the equation based on the Taylor expansion of $\nu'_\epsilon(u)$ at $u = 0$; $\nu'_\epsilon(u) = a_0 + b_0u + O(u^2)$, and at $u = 1$; $\nu'_\epsilon(u) = a_1 + b_1u + O(u^2)$. Note that $b_0 = b_1$, so we call the first order coefficient b from here. This allows us to approximate $\nu'_\epsilon(u)$ in an interval, I_ς , with a linear function, bu . The interval is,

$$I_\varsigma := [0 - \varsigma, 0 + \varsigma] \cup [1 - \varsigma, 1 + \varsigma].$$

Denote a binary function, \tilde{b}^n given by:

$$\tilde{b}_{ij}^n = \begin{cases} b, & \text{if } u_{ij}^n \in I_\varsigma \\ 0, & \text{elsewhere.} \end{cases}$$

Then, with $\tilde{B}^n = \text{diag}(\tau\alpha\tilde{b}^n)$, we can adjust (4.14) as follows:

$$\begin{aligned} u_1^{n+1} &= u_1^n + 2\tau\mu \nabla \cdot \left(\frac{\nabla u_1^{n+1}}{|\nabla u_1^{n+1}|_{\epsilon_2}} \right) - \tau\alpha\tilde{b}^n u_1^{n+1} + \tau\alpha\tilde{b}^n u_1^n + \bar{f}^n \\ (I + \tilde{B}^n - 2\tau\mu A_1(u_1^n)) u_1^{n+1} &= u_1^n + \tau\alpha\tilde{b}^n u_1^n + \bar{f}^n \\ u_1^{n+1} &= \underbrace{(I + \tilde{B}^n - 2\tau\mu A_1(u_1^n))^{-1}}_{Q_1} (u_1^n + \underbrace{\tau\alpha\tilde{b}^n u_1^n + \bar{f}^n}_{f_1}). \end{aligned} \quad (4.15)$$

This scheme improves the performance of AOS_0 because the changes in f_1 (4.15) between iterations is limited, compared to f_0 (4.14). The addition of $\tau\alpha\tilde{b}^n u_1^n - \tau\alpha\tilde{b}^n u_1^{n+1}$ has the effect of approximating the change in ν'_ϵ between n and $n+1$, in I_ς . We call the above scheme AOS_1 (4.15) from here. In Weickert et al. [29] conditions for a discrete scale space were provided, required for convergence. The conditions for $Q(u^n) = (q_{ij}(u^n))$ are as follows, where N is number of pixels and $J := \{1, \dots, N\}$:

(D1) Continuity in its argument:

$$Q \in C(\mathbb{R}^N, \mathbb{R}^{N \times N})$$

(D2) Symmetry:

$$q_{ij} = q_{ji}, \quad \forall i, j \in J$$

(D3) Unit row sum:

$$\sum_{j \in J} q_{ij} = 1, \quad \forall i \in J$$

(D4) Nonnegativity:

$$q_{ij} \geq 0, \quad \forall i, j \in J$$

(D5) Positive diagonal:

$$q_{ii} > 0, \quad \forall i \in J$$

(D6) Irreducibility:

For any $i, j \in J$ there exist $k_0, \dots, k_r \in J$ with $k_0 = i$ and $k_r = j$ such that $q_{k_p k_{p+1}} \neq 0$ for $p = 0, \dots, r - 1$.

The matrix Q_1 (4.15) does not fulfil this criteria, specifically (D2) Symmetry and (D3) Unit row sum. In order to satisfy these conditions, we must first make the following adjustment, compared to (4.15). Again, we only consider the x -direction here:

$$\begin{aligned} u_1^{n+1} &= u_1^n + 2\tau\mu\nabla \cdot \left(\frac{\nabla u_1^{n+1}}{|\nabla u_1^n|_{\epsilon_2}} \right) - \tau\alpha\tilde{b}^n u_1^{n+1} + \tau\alpha\tilde{b}^n u_1^n - \bar{f}^n \\ \left((I + \tilde{B}^n) - 2\tau\mu A_1(u_1^n) \right) u_1^{n+1} &= (I + \tilde{B}^n) u_1^n + \bar{f}^n \\ u_1^{n+1} &= \underbrace{\left(I - 2\tau\mu(I + \tilde{B}^n)^{-1} A_1(u_1^n) \right)^{-1}}_{Q_2} \left(u_1^n + \underbrace{(I + \tilde{B}^n)^{-1} \bar{f}^n}_{f_2} \right). \end{aligned} \tag{4.16}$$

Depending on the choice of ς , there is unit row sum and symmetry in Q_2 (4.16). By increasing ς , such that $\tilde{b} = b$, (D2) and (D3) are fulfilled for AOS_2 . As $u \in [0, 1]$, $\varsigma = 0.5$ is enough to ensure this. This adjustment consists of multiplying τ by a scalar, dependent on b and α . This can be interpreted as automatically setting the time step to $\tilde{\tau}$:

$$\tilde{\tau} = \frac{\tau}{1 + \tau\alpha b}. \tag{4.17}$$

This restricts the size of time step based on the prominence of the penalty function, dictated by the size of α , and represented by b . We will present results for AOS_0 , AOS_1 and AOS_2 in Section 5. For the schemes above (AOS_0 , AOS_1 , AOS_2), as before, the corresponding equation for u_2^{n+1} is solved and then the complete update is given by:

$$u^{n+1} = \frac{u_1^{n+1} + u_2^{n+1}}{2}.$$

4.4.2 The New Algorithm

The algorithm computes a solution for a sequence of alternating minimization problems. For each fixed c_1 and c_2 we have a new minimization problem, which is solved using AOS_0 , AOS_1 or AOS_2 . The final solution, when c_1 and c_2 have converged, is denoted u^* .

Algorithm AOS method for CDSS

- 1: Set μ, θ . Calculate g and P_d using (3.2) and (4.1) respectively.
 - 2: Initialize $u^{(0)}$ such that Γ is the boundary of \mathcal{P} .
 - 3: **for** $k \leftarrow 1 : \text{maxit}$ **do**
 - 4: Calculate $c_1^{(k)}(u^{(k-1)})$ and $c_2^{(k)}(u^{(k-1)})$ using (4.11)
 - 5: Calculate $r_p^{(k)} = \lambda \left((z - c_1^{(k)})^2 - (z - c_2^{(k)})^2 \right) + \theta P_d$.
 - 6: Set $\alpha^{(k)} = \|r_p^{(k)}\|_{L^\infty}$.
 - 7: $u^{(k)} \leftarrow \min_u CDSS \left(c_1^{(k)}, c_2^{(k)}, \alpha^{(k)} \right)$ using AOS scheme.
 - 8: **end for**
 - 9: $u^* \leftarrow u^{(k)}$.
-

5 Experimental Results

This section will show three sets of experiments to test the effectiveness of our new algorithms and to compare them with the existing model. In the following we select the parameters as follows. We have found that setting $\epsilon_1 = 10^{-2}$ produces a tight approximation of $\nu(u)$. We fix the penalty parameter at $\alpha = \|\lambda r + \theta P_d\|_{L^\infty}$, which is enough to enforce the constraint [8]. We set the time step at $\tau = 10^{-2}$ and $\varsigma = 0.1$, except in Test Set 3, where they are varied to demonstrate the benefits of the improved AOS method. The only restriction on ϵ_2 is that it is small; we select it as $\epsilon_2 = 10^{-6}$. We have to consider the balance between the regularization and fitting term, which will change for each problem. Here we set $\lambda = 1$ and vary μ for each problem, depending on the shape and smoothness of the boundary of the desired object. It might be worth considering the work of Mylona et al. [23] who automatically optimize these parameters based on image information. The following tests use only three points input by the user, i.e. $n_1 = 3$. The model is capable of achieving the desired result with a simple shape within the target, even for awkwardly shaped targets as seen in Figs. 3 and 4. The resilience to these selections is discussed further in 5.2. This leaves the main choice for a successful segmentation as the distance selection parameter, θ . In these tests, it varies between 1 and 4.5. The basis for this choice is the size of the target object and its proximity to other image features of similar intensity, and can be intuitively selected quite reliably.

In Test Set 1 results are presented for the proposed **nonconvex** Distance Selective Segmentation (DSS) model and compared to the successful Rada-Chen model [28], demonstrating its robustness in difficult cases, whilst underlining the need for the convex reformulation. In Test Set 2, results are presented for the **Convex** Distance Selective Segmentation (CDSS) model, demonstrating its success in segmentation of a range of examples independently of initialization and its robustness to user input. Test Set 3 demonstrates quantitative improvement of the new AOS method, in relation to one example. All images tested are of size 128x128.

5.1 Test Set 1 – comparisons of two nonconvex models

In Fig. 1 results are presented for three examples for Rada-Chen [28] and in Fig. 2 the same examples are presented for DSS. Results demonstrate that the new model can also produce

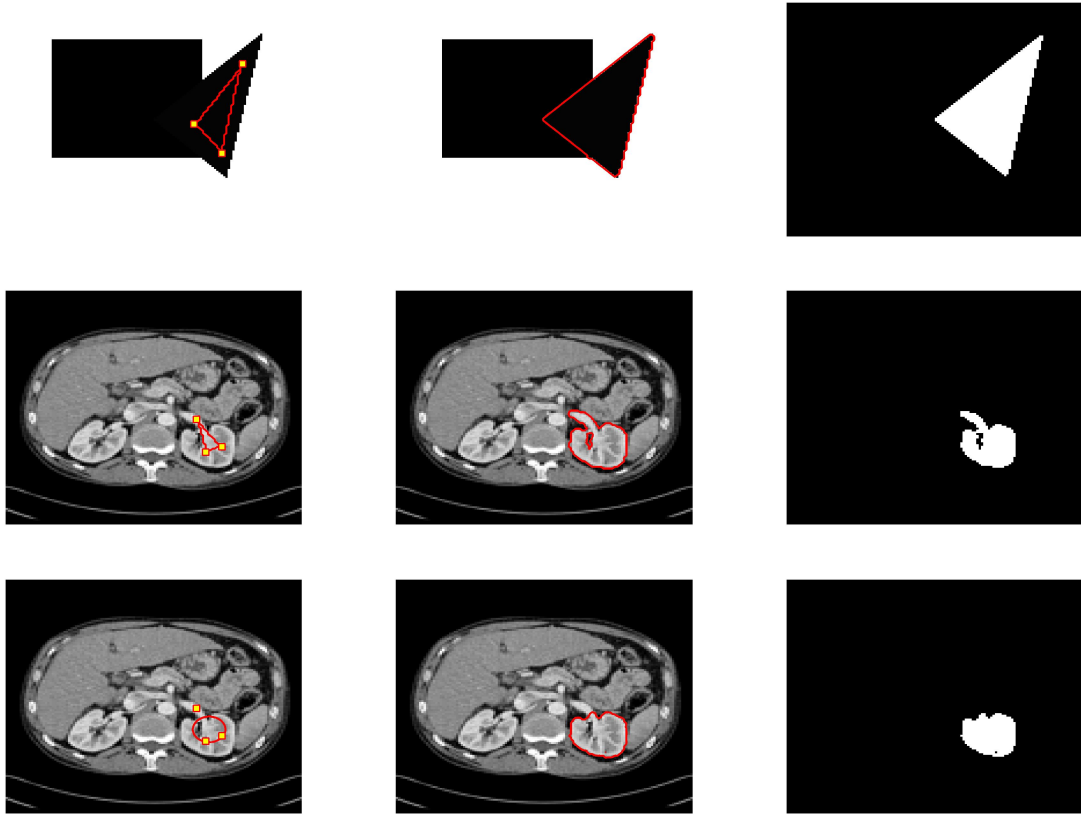


Figure 1: Results for Rada-Chen [28], for three test problems (given by rows 1-3). From left to right: initialization (with user input set \mathcal{A}), final contour, object selected

the successful results of Rada-Chen [28], whilst both models are sensitive to initialization, as evident in row 3 of each figure. The nature of the failure in each case is due to finding a local minimum, as is possible for the nonconvex formulation. This is evident from the fact that the user input set, \mathcal{A} , is the same for rows 2 and 3 whilst the initializations are different, and one case fails where as the other succeeds. This provides the motivation for convexifying the energy in the DSS case, as this cause of failure is removed.

5.2 Test Set 2 – demonstration of independence of initialization of CDSS

In Fig. 3 results for CDSS are presented for three examples. The function is initialized as the given image, with successful segmentation in each case. In Figs. 4 and 5 the same object is selected, with different user input for each. The solution (ground truth) is given by an ideal user input set, \mathcal{A}^* , which is the shape of the target object and would require n_1 to be large. This is not feasible in practice, as it essentially consists of a manual segmentation. We intend to demonstrate that an acceptable approximation of the solution can be achieved with only three points ($n_1 = 3$), even when segmenting a difficult shape. We have two choices of user

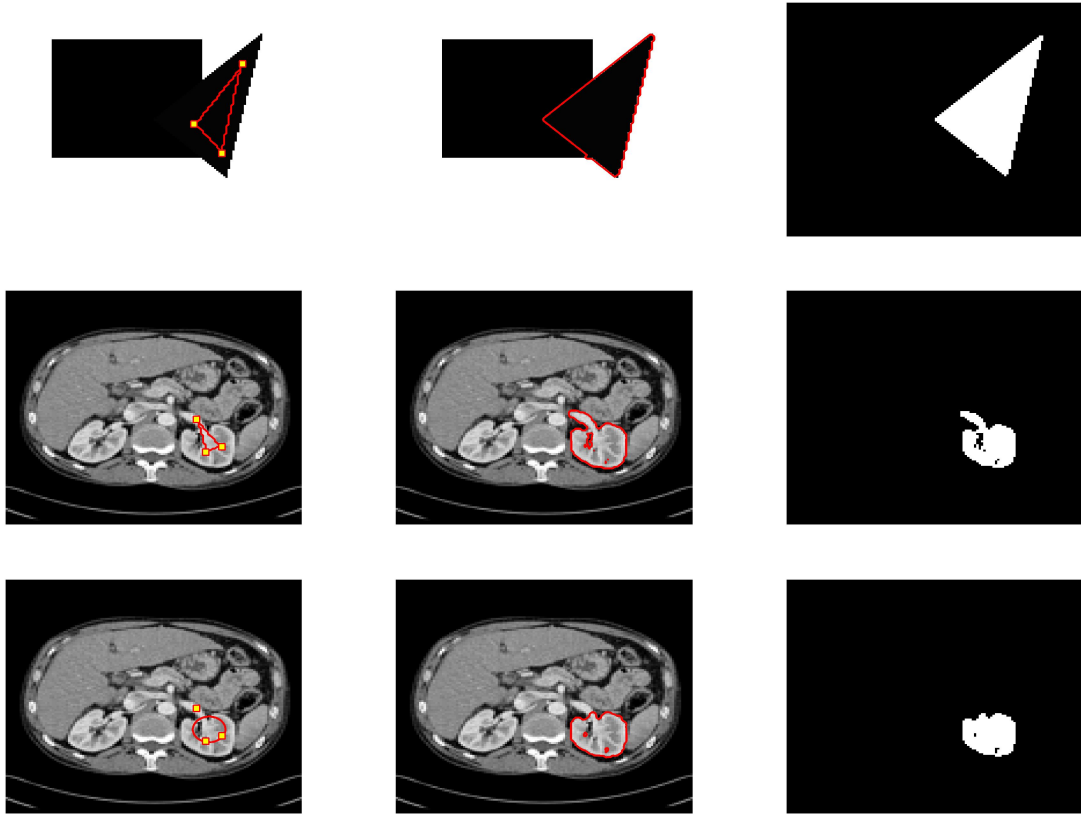


Figure 2: Results for DSS, for three test problems (given by rows 1-3). From left to right: initialization (with user input set \mathcal{A}), final contour, object selected

input, \mathcal{A}_4 from Fig. 4 and \mathcal{A}_5 from Figure 5. Whilst \mathcal{A}_5 is close to the boundary of the target (and closer to the ideal user input, \mathcal{A}^*), \mathcal{A}_4 is a more interior selection. These produce slightly different results, but both are acceptable. This demonstrates that even with a simple user input far from the ideal, such as \mathcal{A}_4 , we get an acceptable result. A more appropriate user input (i.e. closer to the ideal), such as \mathcal{A}_5 , produces a better result, but still only requires three points. One observes that the initializations were deliberately chosen to be not within the object intended (which would fail with all other nonconvex models) and yet CDSS "knows" where the intended object is and finds it correctly. These examples demonstrate the robustness of the model; successful segmentation is possible for a wide range of user input.

5.3 Test Set 3 – demonstration of effectiveness of the new AOS algorithm

In Fig. 6 the residual is shown for AOS_0 for two different time steps; $\tau = 10^{-2}$ and $\tau = 10^{-3}$. It demonstrates that for a stable convergence, the time step is limited to $\tau = 10^{-3}$. In Fig. 7 the residual is shown for AOS_1 for $\tau = 10^{-2}$ for two different choices of the restriction parameter; $\varsigma = 0.01$ and $\varsigma = 0.1$. It demonstrates that the improved AOS (AOS_1) can achieve stable

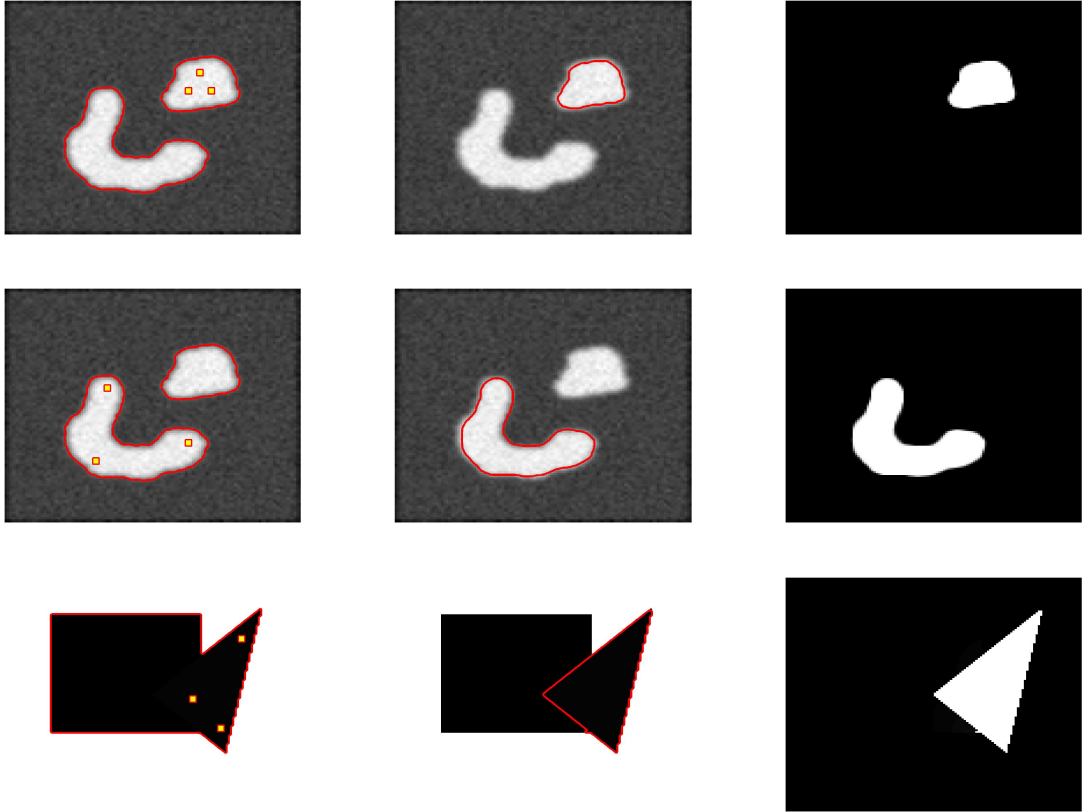


Figure 3: Results for CDSS, for three test problems (given by rows 1-3). From left to right: initialization (with user input set \mathcal{A}), final contour, object selected.

convergence for a higher time step than original AOS (AOS_0), for an appropriate selection of ς . In Fig. 8 the residual is shown for AOS_1 for $\tau = 10^{-1}$ for two different choices of the restriction parameter; $\varsigma = 0.1$ and $\varsigma = 0.5$. It demonstrates that the improved AOS (AOS_1) can achieve stable convergence for higher time steps, depending on the selection of ς . We have found that the fastest stable convergence is for $\tau = 10^{-2}, \varsigma = 0.1$.

In Fig. 9 the residual is shown for AOS_2 for $\tau = 1$ for two different choices of the restriction parameter; $\varsigma = 0.1$ and $\varsigma = 0.5$. It demonstrates that AOS_2 can achieve stable convergence for a higher time step than AOS_0 and AOS_1 , for an appropriate selection of ς , i.e. $\tilde{b} = b$. This scheme (AOS_2) complies with the discrete scale space conditions [29] for $\varsigma = 0.5$, and has stable convergence for large time steps. It can be seen as a variable time step, given by $\tilde{\tau}$ (4.17), dependent on the contribution of the penalty term.

Further improvements in the computational speed of minimizing CDSS can be explored by applying recent optimization techniques, developed to efficiently solve convex optimization problems in imaging. These include the Split Bregman method, applied to convex segmentation problems by Goldstein et al. [12]; Chambolle et al. [7] introduced a fast primal dual algorithm

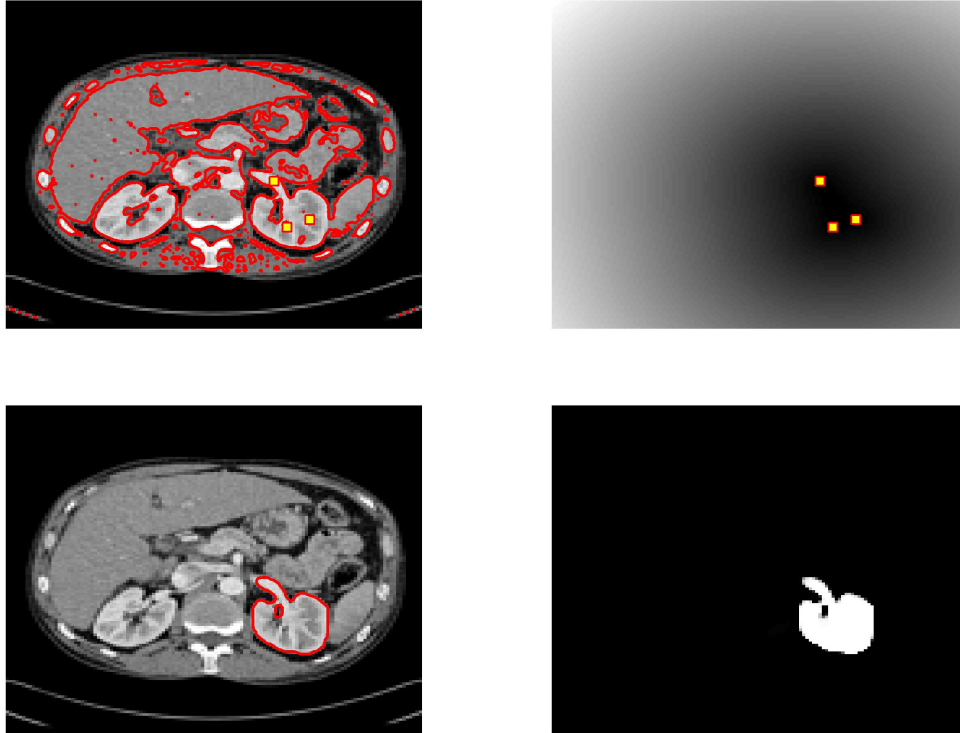


Figure 4: User input set 1 for CDSS. From left to right, top to bottom: initialization, P_d function (with user input set \mathcal{A}_4), final contour, object selected.

applicable to convex segmentation; and Yuan et al. [30] introduced a max flow based algorithm for binary labelling problems. These methods would further improve the results for CDSS, in terms of computational efficiency.

6 Conclusions

In this paper we discussed the drawbacks of current selective segmentation models and proposed a new model where a global minimizer can be found independently of initialization. The results presented show that the proposed model is reliable and efficient in a wide range of examples and is not sensitive to user input. We have also introduced improvements to the AOS scheme used in previous selection models [1, 2, 27, 28], based on the Taylor expansion of our proposed penalty function. These demonstrate improved reliability, and an improvement in computational speed.

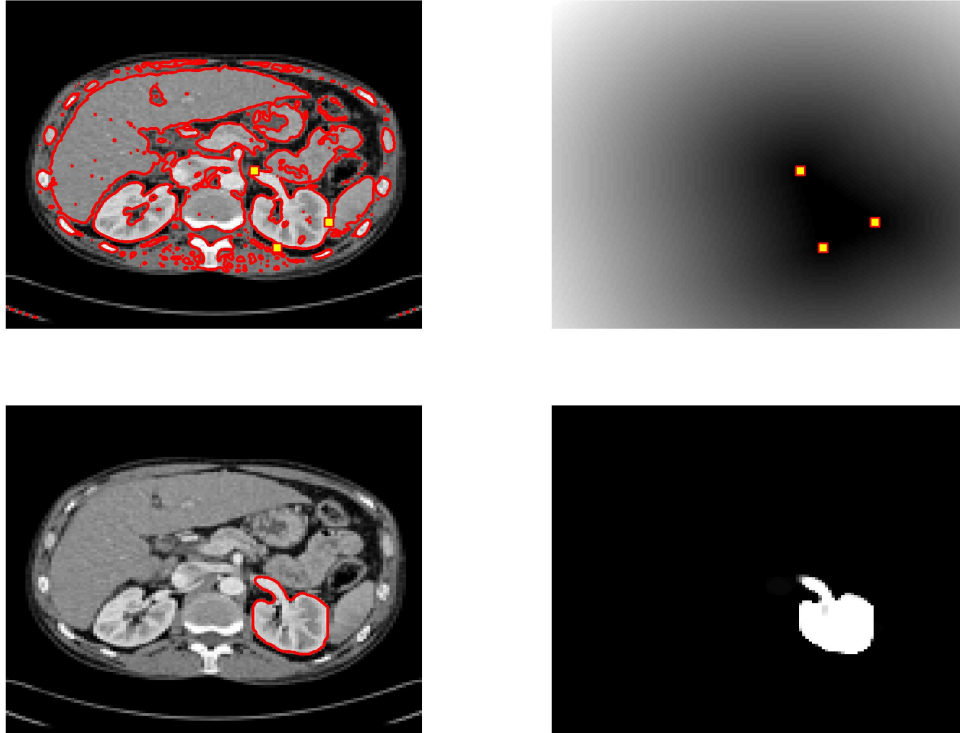


Figure 5: User input set 2 for CDSS. From left to right, top to bottom: initialization, P_d function (with user input set \mathcal{A}_5), final contour, object selected.

References

- [1] N. Badshah and K. Chen. Image selective segmentation under geometrical constraints using an active contour approach. *Commun. Comput. Phys.*, 7(4):759–778, 2009.
- [2] N. Badshah, K. Chen, H. Ali, and G. Murtaza. Coefficient of variation based image selective segmentation model using active contours. *East Asian Journal on Applied Mathematics*, 2:150–169, 2012.
- [3] E. Bae, J. Yuan, and X. C. Tai. Global minimization for continuous multiphase partitioning problems using a dual approach. *Int. J. Computer Vision*, 92:112–129, 2011.
- [4] X. Bresson, S. Esedoglu, P. Vandergheynst, J. P. Thiran, and S. Osher. Fast global minimization of the active contour/snake model. *J. Math. Imaging Vis.*, 28:151–167, 2007.
- [5] V. Caselles, R. Kimmel, and G. Sapiro. Geodesic active contours. *International Journal of Computer Vision*, 22(1):61–79, 1997.
- [6] A. Chambolle, D. Cremers, and T. Pock. A convex approach to minimal partitions. *SIAM Journal on Imaging Sciences*, 5(4):1113–1158, 2012.

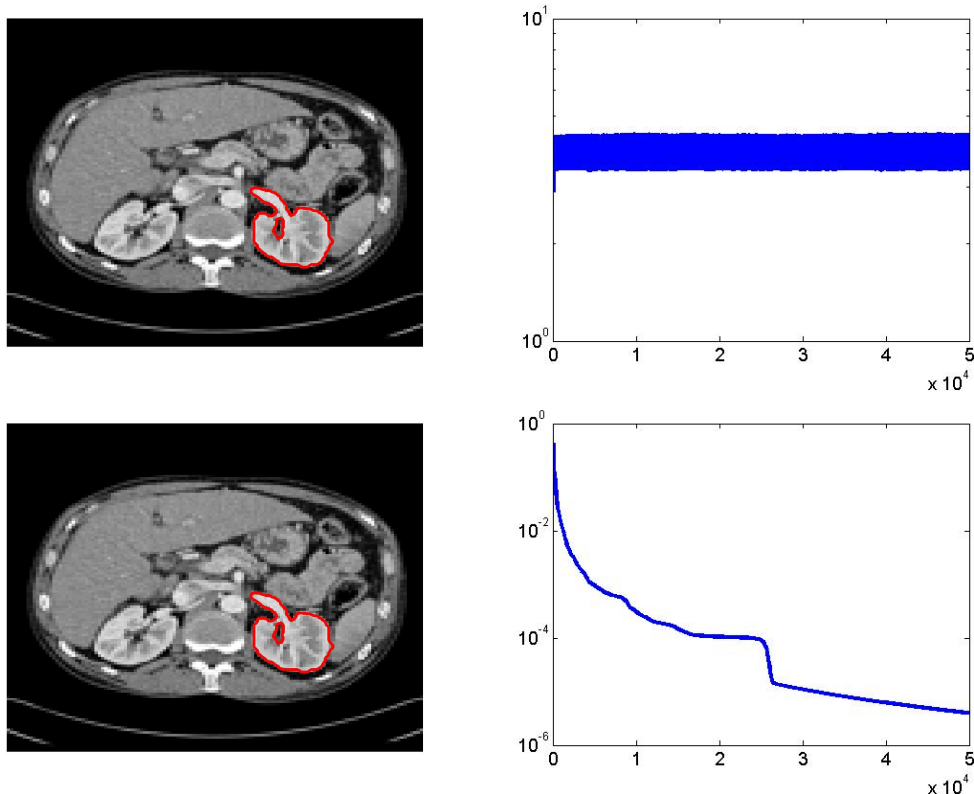


Figure 6: Results for AOS_0 for CDSS. Row 1 is for $\tau = 10^{-2}$, row 2 is for $\tau = 10^{-3}$. From left to right: final contour and residual for u (with number of iterations).

- [7] A. Chambolle and T. Pock. A first-order primal-dual algorithm for convex problems with applications to imaging. *Journal of Mathematical Imaging and Vision*, 40:120–145, 2011.
- [8] T. F. Chan, S. Esedoglu, and M. Nikolova. Algorithms for finding global minimizers of image segmentation and denoising models. *SIAM Journal on Applied Mathematics*, 66:1932–1648, 2006.
- [9] T. F. Chan and J. H. Shen. *Image Processing and Analysis - Variational, PDE, Wavelet, and Stochastic Methods*. SIAM Publications, Philadelphia, USA, 2005.
- [10] T. F. Chan and L. Vese. Active contours without edges. *IEEE Transactions on Image Processing*, 10(2):266–277, 2001.
- [11] E. Giusti. *Minimal Surfaces and Functions of Bounded Variation*. Birkhauser Boston, 1984.
- [12] T. Goldstein, X. Bresson, and S. Osher. Geometric applications of the split bregman method. *Journal of Scientific Computing*, 45:272–293, 2010.

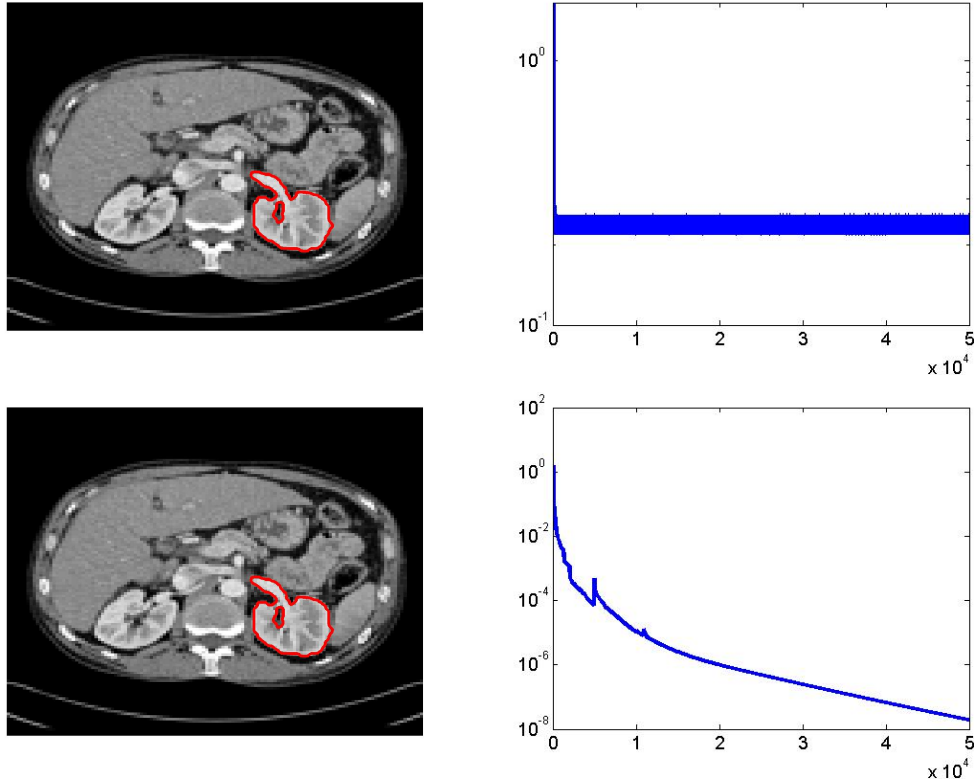


Figure 7: Results for $AOS_1, \tau = 10^{-2}$ for CDSS. Row 1 is for $\zeta = 0.01$, row 2 is for $\zeta = 0.1$. From left to right: final contour and residual for u (with number of iterations).

- [13] C. Gout and C. Le Guyader. Geodesic active contour under geometrical conditions theory and 3d applications. *Numerical Algorithms*, 48:105–133, 2008.
- [14] C. Gout, C. Le Guyader, and L. Vese. Segmentation under geometrical conditions with geodesic active contour and interpolation using level set method. *Numerical Algorithms*, 39:155–173, 2005.
- [15] Y. Gu, L. L. Wang, and X. C. Tai. A direct approach towards global minimization for multiphase labeling and segmentation problems. *IEEE Transactions on Image Processing*, 21:2399 – 2411, 2012.
- [16] J. B. Hiriart-Urruty and C. Lemarechal. *Convex Analysis and Minimization Algorithms. I. Fundamentals*. Grundlehren Math. Wiss. 305. Springer-Verlag, New York, 1993.
- [17] M. Kass, A. Witkin, and D. Terzopoulos. Snakes: active contour models. *International Journal of Computer Vision*, 1(4):321–331, 1988.

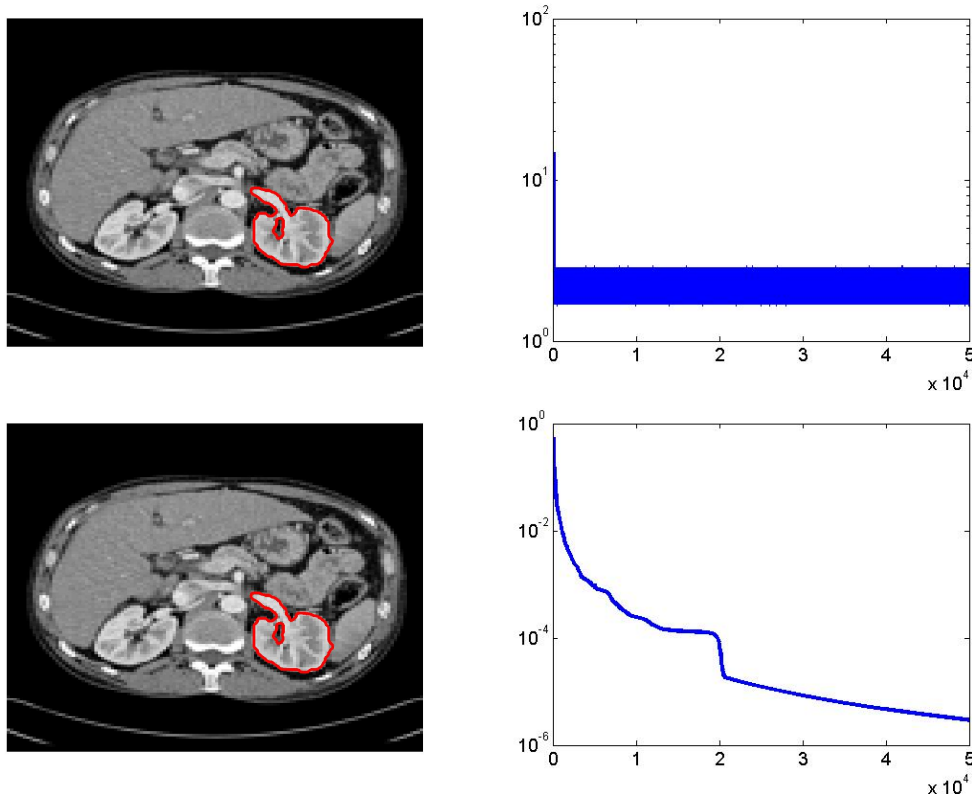


Figure 8: Results for $AOS_1, \tau = 10^{-1}$ for CDSS. Row 1 is for $\zeta = 0.1$, row 2 is for $\zeta = 0.5$. From left to right: final contour and residual for u (with number of iterations).

- [18] J. Lellmann, F. Becker, and C. Schnörr. Convex optimization for multi-class image labeling with a novel family of total variation based regularizers. In *IEEE International Conference on Computer Vision (ICCV)*, 2009.
- [19] C. Li, C. Xu, C. Gui, and M. D. Fox. Level set evolution without re-initialization: A new variational formulation. *IEEE Computer Society Conference on Computer Vision and Pattern Recognition*, 1:430–436, 2005.
- [20] T. Lu, P. Neittaanmaki, and X. C. Tai. A parallel splitting-up method for partial differential equations and its application to navier-stokes equations. *RAIRO Math. Mod. Numer. Anal.*, 26(6):673–708, 1992.
- [21] A. Mitiche and I. Ben-Ayed. *Variational and Level Set Methods in Image Segmentation*. Springer Topics in Signal Processing. Springer, 2010.
- [22] D. Mumford and J. Shah. Optimal approximation by piecewise smooth functions and associated variational problems. *Comm. Pure Appl. Math.*, 42:577–685, 1989.

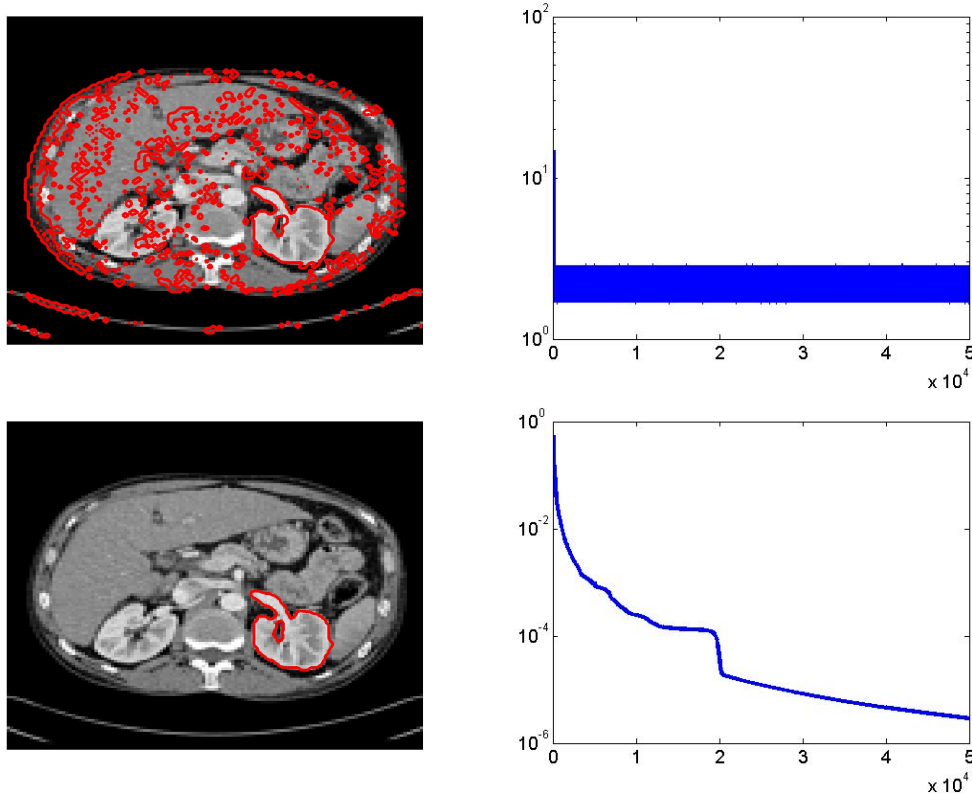


Figure 9: Results for $AOS_2, \tau = 1$ for CDSS. Row 1 is for $\zeta = 0.1$, row 2 is for $\zeta = 0.5$. From left to right: final contour and residual for u (with number of iterations).

- [23] E. Mylona, M. Savelonas, and D. Maroulis. Automated adjustment of region-based active contour parameters using local image geometry. *IEEE Transactions on cybernetics*, 2014. to appear.
- [24] M. Ng, G. Qiu, and A. Yip. Numerical methods for interactive multiple class image segmentation problems. *Int. J. Imaging Systems and Technology*, 20:191–201, 2010.
- [25] T. Nguyen, J. Cai, J. Zhang, and J. Zheng. Robust interactive image segmentation using convex active contours. *IEEE Transactions on Image Processing*, 21:3734–3743, 2012.
- [26] S. Osher and J. Sethian. Fronts propagating with curvature-dependent speed: algorithms based on Hamilton-Jacobi formulations. *J. Computational Physics*, 79(1):12–49, 1988.
- [27] L. Rada and K. Chen. A new variational model with dual level set functions for selective segmentation. *Commun. Comput. Physics*, 12(1):261–283, 2012.
- [28] L. Rada and K. Chen. Improved selective segmentation model using one level-set. *Journal of Algorithms & Computational Technology*, 7(4):509–540, 2013.

- [29] J. Weickert, B. M. ter Haar Romeny, and Max A. Viergever. Efficient and reliable schemes for nonlinear diffusion filtering. *IEEE Transactions on Image Processing*, 7:398–410, 1998.
- [30] J. Yuan, E. Bae, X.C. Tai, and Y. Boykov. A spatially continuous max-flow and min-cut framework for binary labeling problems. *Numerische Mathematik*, 126(3):559–587, 2014.
- [31] J. P. Zhang, K. Chen, and B. Yu. A 3D multigrid algorithm for the Chan-Vese model of variational image segmentation. *Int. Journal of Computer Math.*, 89:160–189, 2012.
- [32] Y. L. Zheng and K. Chen. A hierarchical algorithm for multiphase texture image segmentation. *ISRN Signal Processing*, 781653:1–11, 2012.